

Chapter 5

Preparation and characterization of chitosan/bentonite and chitosan/silica clay biocomposites and a comparative study with chitosan/kaolin clay biocomposites

(M. Bhattacharjee, S. Goswami, N. B. Pramanik, J. Barman, M. Saikia, N. R. S. Hulle, D. J. Haloi;

Analytical Chemistry Letters 13, 609-625, 2023)

Abstract

In this work, we report the preparation of CS/BNTN and CS/SIO biocomposite films and characterizations of those via various analytical techniques such as FT-IR, UV/Vis, XRD, SEM, UTM, TGA and DSC. The synthesized biocomposite films exhibit appreciable antimicrobial activity against *Escherichia coli* and *Bacillus subtilis* bacteria using the agar well diffusion method. Swelling tests of prepared biocomposite films were also carried out in distilled water to evaluate their property towards packaging applications. Additionally, it has been noted that compared to the films of the other two biocomposites, the CS/BNTN biocomposite films showed greater tensile strength, swelling capacity and antimicrobial activity.

5.1. Introduction

In recent decades, biodegradable polymers have been greatly emphasized for their excellent applications in several industries due to their fascinating properties [147]. Among those, CS is one of the most promising biodegradable polymers [148]. The chemical modifications of the CS framework drastically enhance the physicochemical properties. Various biocomposites of CS are synthesized using different chemical functionality. This methodology escalates to creating some novel materials of the same with exciting characteristics. Basically, CS-based biocomposites are prepared by using different types of inorganic substances such as layered silicates. Only CS-based products are rare as they don't have characteristics similar to that of CS-biocomposite materials. In the last few years, many CS-based biocomposites were developed to help with environmental challenges. For this reason, CS immobilization on clay minerals has gained serious attention for various applications [67].

Various studies revealed that clay minerals as naturally occurring inorganic compounds with unique structural adsorption, rheological, and thermal characteristics [137]. These materials are inherently hydrophilic in nature due to the presence of -OH groups on their surface, which may readily form bonds with water molecules [138]. On very few occasions purification and modification are required to increase the clay's compatibility with other polymers [141]. Clay minerals significantly improve the characteristics of CS which are due to their smaller particle size, high surface area, favourable aspect ratio, and better dispersion ability. The implementations of clay minerals in the industries of food, pharmaceutical, cosmetic, and other areas can be a result of various properties of clay viz. biocompatibility,

non-toxicity, and outstanding controlled release ability [39]. The most incorporated silicate in polymer composites is BNTN clay. It is an aluminosilicate of 2:1 type and is made up of recurring triple-layer sheets with a thickness of about 1 nm and a length between hundred to several hundred nanometers that is shared by two tetrahedral silica sheets and an octahedral sheet of alumina [149]. When layers are stacked over one other, a space between them is created which is referred to as the interlayer. Weak electrostatic forces hold these parallel layers together to make the entire structure. The cations inside the interlayer can be easily transferred by other cations as it holds weak interaction between the stacking layers [69]. Another clay with a characteristic porous inorganic morphology with significant pore volume, varied pore structure and high surface area is SIO. It is also used as support and in some modification techniques of other materials. Moreover, SIO is very much applicable to various industries like rubber, pesticides, papermaking, plastic processing, etc. [52, 53].

The electrolytic and chelating nature of CS is characterized by the presence of the acidity of the $-NH_3^+$ group. Moreover, due to its polycationic nature in acidic environments, CS may be intercalated in the different clays through the cationic exchange mechanism and hydrogen bonding interactions. Thus, the biocomposite form demonstrates intriguing structural and functional traits [45, 69]. Recent literature reveals detailed the several characteristics and applications of these hybrid materials of clay and CS [45, 53, 69, 77-79, 91-93, 150].

The main goal of our current investigation is to prepare CS/clay biocomposite films by combining BNTN and SIO clay with an acidified aqueous solution of CS. A few biocomposite films using two different kinds of clay viz. BNTN and SIO are prepared by the method explained in the chapter 4 and the results are also compared with that report of CS/KAO biocomposite films. Various physicochemical methods, including FT-IR, UV/Vis, XRD, SEM, UTM, TGA, and DSC are used to characterize these synthesized CS/clay biocomposite films. Notable antimicrobial activity of these biocomposite films was observed against two bacteria - *Escherichia coli* and *Bacillus subtilis*. Swelling tests are performed for these biocomposite films. To the extent that we are aware, there has not been comparative research done for different CS/clay biocomposite films. Moreover, there has been no investigation carried out on the swelling tests of CS/SIO biocomposite films. Aside from that, the antimicrobial activity of those materials for *Escherichia Coli* and *Bacillus subtilis* bacteria has never been reported. We strongly believe that swelling property investigation, biological applicability and comparative analysis of various physicochemical characteristics of CS/clay biocomposite films make our work a novel and applicable one for

diversified areas. We are thus very much interested in synthesizing these green bio-composite materials based on CS and clay material which are bio-friendly and non-hazardous to the environment. We believe that there are several aspects yet to be explored in this area, and our investigation is just a breakthrough in this domain.

5.2. Synthesis

5.2.1. Chitosan/clay biocomposite films

First 100 mL of 2% aqueous acetic acid solution were used to dissolve 1 g of CS powder. This mixture was subsequently agitated at a temperature of 40 °C for a duration of 5 h. The resulting CS solution was then combined with 0.1 g of BNTN clay while being agitated at room temperature for 24 h at a speed of roughly 700 rpm. Subsequently, the resultant solution was poured into a petri dish and subjected to a 24 h drying period at 60 °C to facilitate the evaporation of the solvent, ultimately yielded the biocomposite films. To eliminate any remaining acetic acid residue, the film was immersed in an aqueous solution containing 0.05 M NaOH. Following this, the film underwent neutralization by rinsing it with distilled water and was then allowed to air dry at room temperature. The similar procedure was applied for the synthesis of CS/SIO clay biocomposite films. The details of preparative data of CS/clay biocomposite films are shown in Table 5.1. CS/BNTN clay biocomposite films with 10% and 30% of BNTN clay are denoted as CS/BNTN-1 and CS/BNTN-3 respectively, whereas CS/Si biocomposite films with 10% and 30% of SIO clay are denoted as CS/SIO-1 and CS/SIO-3 respectively.

The prepared CS/clay biocomposite films with different physical parameters are shown in Table 5.1 and Figure 5.1.

Table 5.1. The preparative data of CS/clay biocomposite films.

Sample	Film thickness (mm)	Amount of CS in g	Clay used	Clay % w. r. t. the amount of CS
CS/BNTN-1	0.15	1	BNTN	10
CS/BNTN-3	0.18	1	BNTN	30
CS/SIO-1	0.14	1	SIO	10
CS/SIO-3	0.18	1	SIO	30

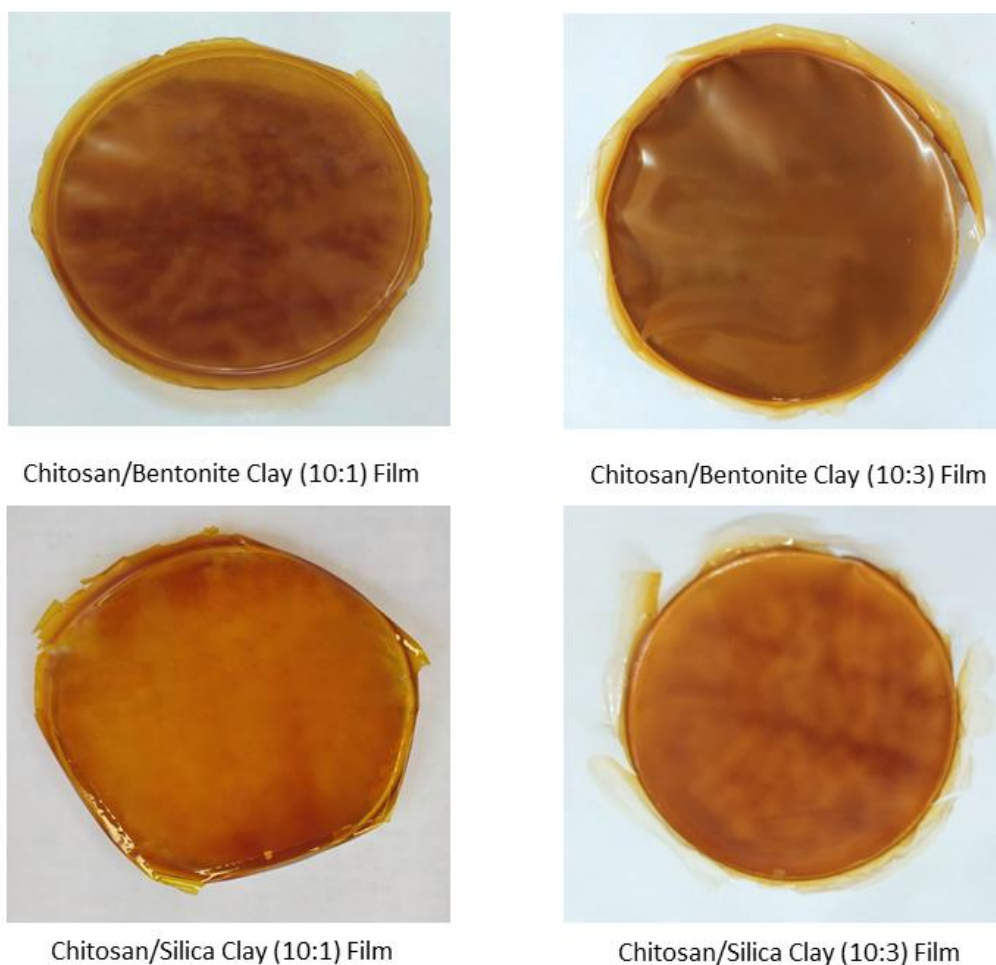


Figure 5.1. Biocomposite films made of CS and clay.

5.2.2. Crude sample for antibacterial study

The preparation of crude sample for antibacterial study is discussed in chapter 4 section 4.2.3.

5.3. Results and discussion

5.3.1. Structural evaluation

5.3.1.1. Analysis via FT-IR spectroscopy

The FT-IR spectra were recorded for the synthesized biocomposites films i.e., CS/BNTN and CS/SIO in the ratios of 10:01 and 10:03 at the region of $4000-700\text{ cm}^{-1}$ (Figure 5.2.). The bands at 3630 , 3433 , 1638 , 994 , and 797 cm^{-1} in Figure 5.2.(a) and Figure 5.2.(b) correspond to the vibrational bands of the silicate which stay unaffected in the biocomposite

films. The additional bands in the biocomposites at 2927 and 1382 cm^{-1} , are consistent with those observed in the pure CS film [69]. The band at 3439 cm^{-1} in Figure 5.2.(c) and Figure 5.2.(d) is the result of stretching vibrations of -OH groups attached to the carbon atom. C-H stretching vibrations arise with intense absorption bands at 2927 cm^{-1} and bending vibrations arise with intense bands at 1415 and 1382 cm^{-1} [51]. The vibration bands at 1532 cm^{-1} in all of the biocomposite films show the electrostatic interaction between the $-\text{NH}_3^+$ group of CS and the negatively charged sites in the added clay. The obtained results are in close agreement with the CS-based hybrid materials [69, 94]. We have thoroughly discussed the FT-IR results of CS and CS/KAO biocomposite films in the chapter 4. When all the biocomposite films are compared with different clay materials (viz. KAO, BNTN, and SIO), it is observed that the vibration band that corresponds to the deformation vibration of the charged amine group in the CS film is found to be shifted towards more low-frequency values in the biocomposite films. This evidence confirmed that the films thus synthesized are not a physical mixture of CS and clay particles; in fact, these are biocomposite films [34].

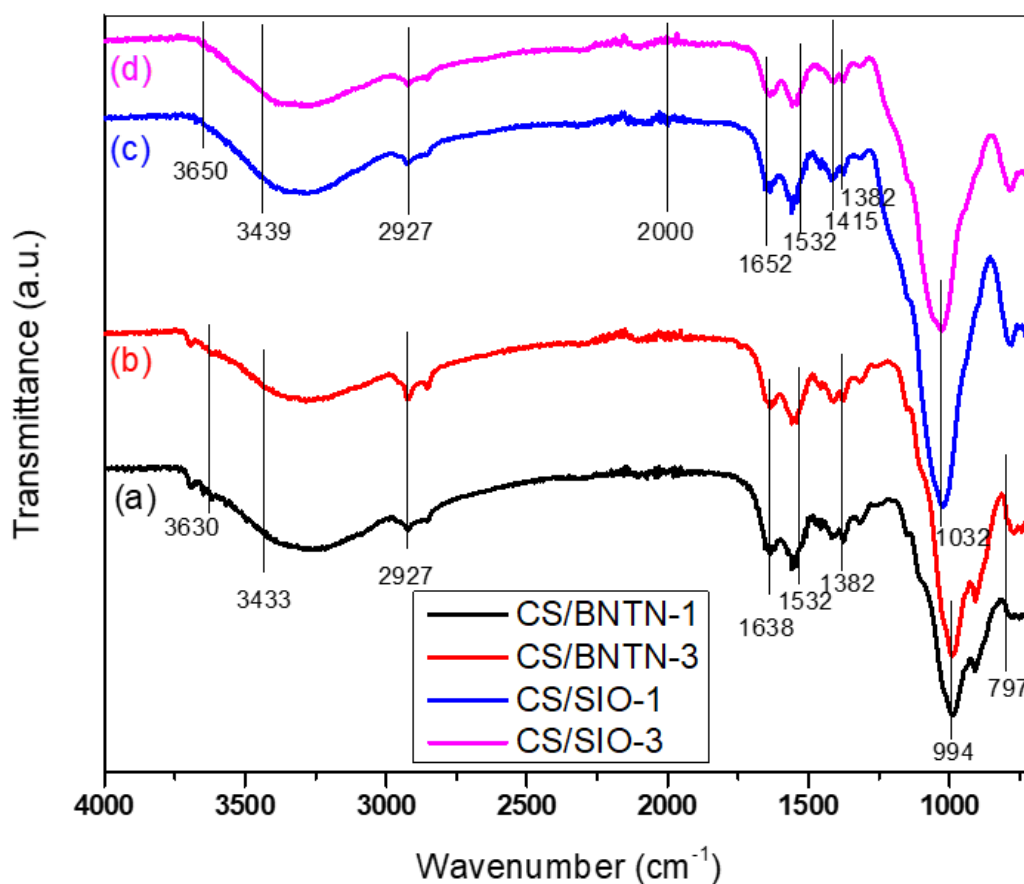


Figure 5.2. FT-IR spectra of different biocomposite films composed of CS and clay.

5.3.1.2. Analysis via UV/Vis spectroscopy

Figure 5.3 displays the UV-Vis spectra of CS/clay biocomposite films that were recorded at ambient temperature. The absorption bands for synthesized biocomposite films were visible between 200-800 nm. Maximum wavelengths for films viz. CS/BNTN-1, CS/BNTN-3, CS/SIO-1, and CS/SIO-3 are obtained at 388 nm, 374 nm, 358 nm and 380 nm, respectively. The absorption bands observed at the range of 300-400 nm are mostly responsible for the direct electronic transition from $d-\pi^*$ orbital which is also termed the Soret band [151]. The position and shape of the UV absorption band were affected by the amount of clay introduced to CS. The variations in the intensity of the absorbed light were closely associated with the increase in the amount of clay in the biocomposite films. When clay particles get concentrated, the molecular interaction occurs as a result the alteration in the shape and position of the bands takes place. Therefore, the peak shifting was observed in various CS/clay biocomposite films. Absorption parameter includes the maximum absorption wavelength (λ_{\max}), absorption intensity and peak shape in the absorption spectrum. Maximum absorption indicates the wavelength where the biocomposite absorbs light most strongly. Shifts in λ_{\max} can signal changes in the interaction between CS and clay. In the chapter 4 we reported that CS shows λ_{\max} value at 354 nm and in the case of all the other CS/clay biocomposite films, the λ_{\max} value shifts towards longer wavelengths which may be corroborated with the enhanced interaction in the biocomposites' electronic structure. Moreover, absorption intensity changes with concentration or the extent of interaction between components. An increase in intensity also indicates enhanced interaction. By comparing CS/BNTN and CS/SIO biocomposite films with CS/KAO clay biocomposite films discussed in chapter 4, it was observed that in all the cases maximum absorption was shown by the biocomposite films which contained the highest concentration of clay. Among all the biocomposite films CS/KAO-3 and CS/BNTN-3 showed maximum absorption (both the values are almost similar). The fact behind the observation may be due to the amount of clay particles in the biocomposite films and the path length it travels. We primarily want to investigate the interaction of various clays with the pure CS molecule from the UV/Vis study. In addition, we were interested in examining how various biocomposite films influence the shape and position of the absorption band. The Soret band at 300-400 nm, which was clearly visible for all the synthesized films, is another goal of this investigation. Therefore, in addition to FT-IR analysis, this analysis also provided strong supporting structural information.

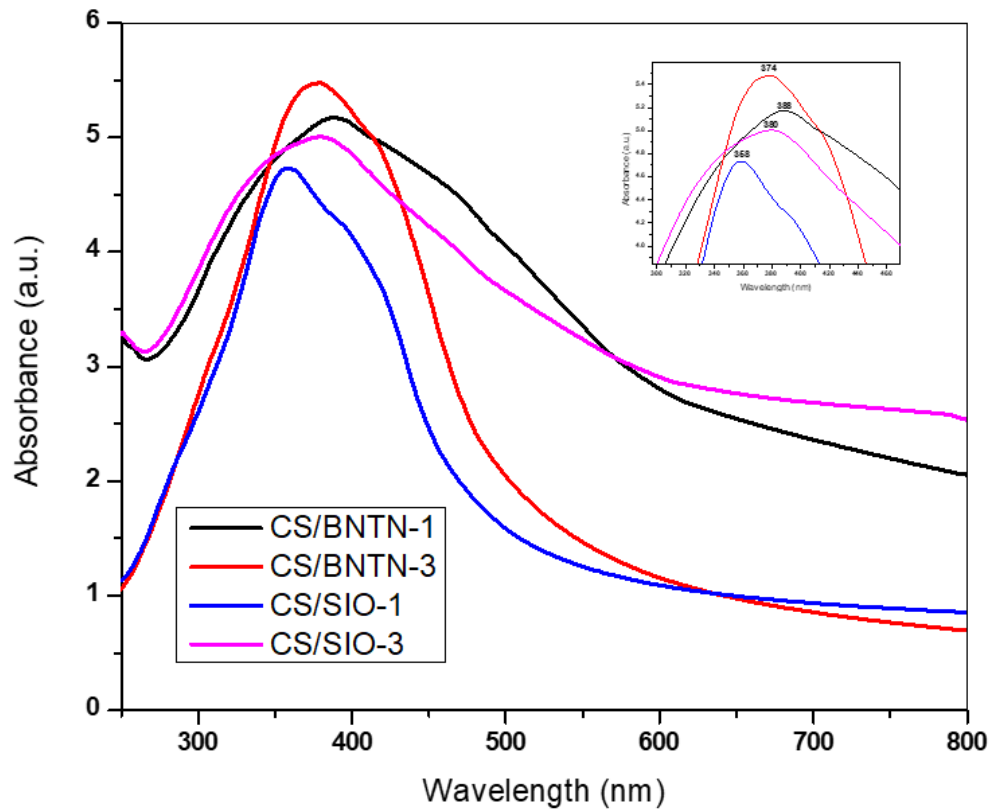


Figure 5.3. UV/Vis spectra of different biocomposite films composed of CS and clay.

5.3.2. Morphological study

5.3.2.1. Analysis via XRD

Figure 5.4.(a) depicts the results of an investigation of the XRD study of the CS/clay biocomposite films. The intense peaks obtained for CS/BNTN and CS/SIO biocomposite films were compared with CS/KAO biocomposite films reported in chapter 4 to know the preliminary information about the incorporation of BNTN and SIO clay in the CS. CS has been shown to have semi-crystalline character whereas BNTN clay is crystalline and SIO clay is amorphous. All the outcomes were noted in the 2θ range, which is around 10° - 70° . For CS/BNTN clay biocomposite films, several intense peaks were observed; however, no such peaks were seen for CS/SIO biocomposite films, which was mostly due to the amorphous nature of the SIO clay. The XRD pattern of CS revealed a large diffraction peak at about 22.4° reported in chapter 4, which corresponds to the usual fingerprints of the semicrystalline nature of CS. The absence of the peak at 22.4° in the CS/clay biocomposite films, as can be seen in Figure 5.4.(a), indicates that the CS in those biocomposite films has lost its crystallinity. It was found that the intensities of the peaks increased as well as a slight

broadening in the biocomposite films from CS/BNTN-1 to CS/BNTN-3 with increasing concentrations of BNTN clay particles. On the other hand, the diffraction peak at 2θ around 22.4° weakened with an increase in the SIO clay percentage in the XRD patterns of CS/SIO-1 and CS/SIO-3. This might be due to the addition of SIO clay which destroyed the hydrogen bond between the CS molecules and thus affected the crystalline structure of CS [53]. Therefore, it can be assumed that all the clays were successfully incorporated into the CS. It was observed that more characteristic peaks were observed in CS/BNTN clay than in CS/KAO biocomposite films and no such distinguish characteristic peaks were observed in the case of CS/SIO clay biocomposite film. This finding indicates that the crystallinity of biocomposite films is arranged as follows:

$$\text{CS/BNTN} > \text{CS/KAO} > \text{CS/SIO}$$

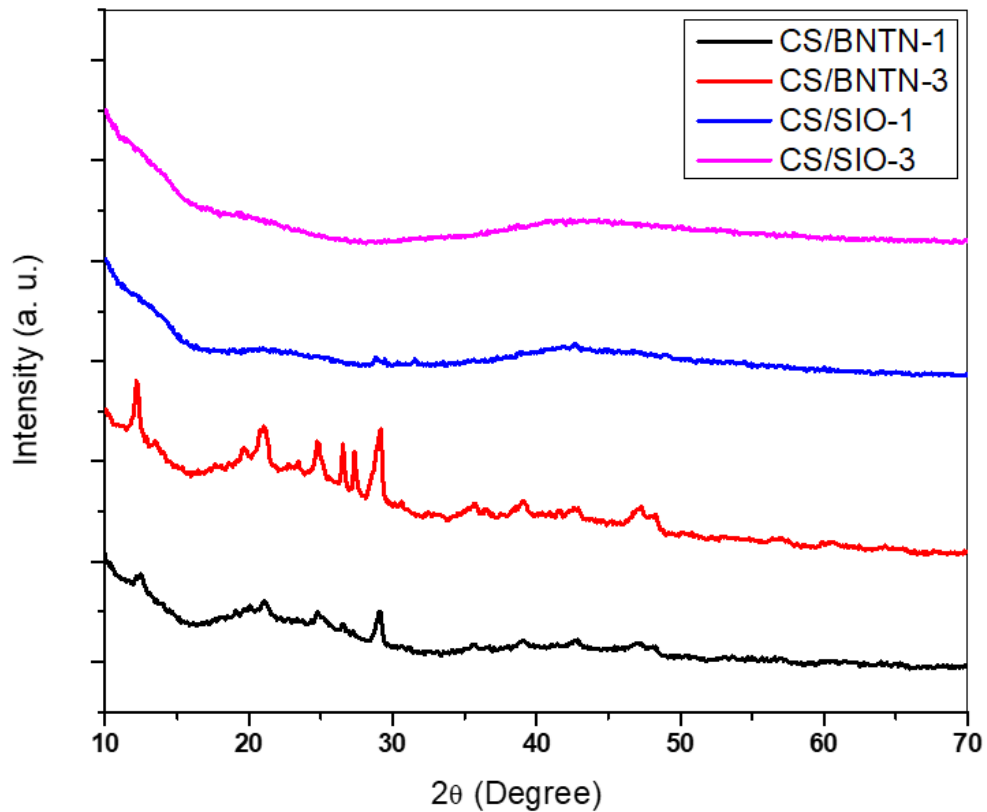


Figure 5.4. (a) XRD patterns of different biocomposite films comprising CS and Clay.

Using the Debye-Scherrer equation (Equation 4.1.), the average crystallite size was determined. For all of the samples, the average value shifts from 18.08 to 19.83 nm. The particle sizes decrease and peaks are slightly shifted to a greater diffraction angle as the clay particle concentration rises. For the purpose of removing the strain caused by the integration of CS, the lattice constant was computed from three significant peaks by the Nelson and

Riley plot, and an average value of 5.3912 \AA was found. Figure 5.4.(b) shows the Nelson Riley plot.

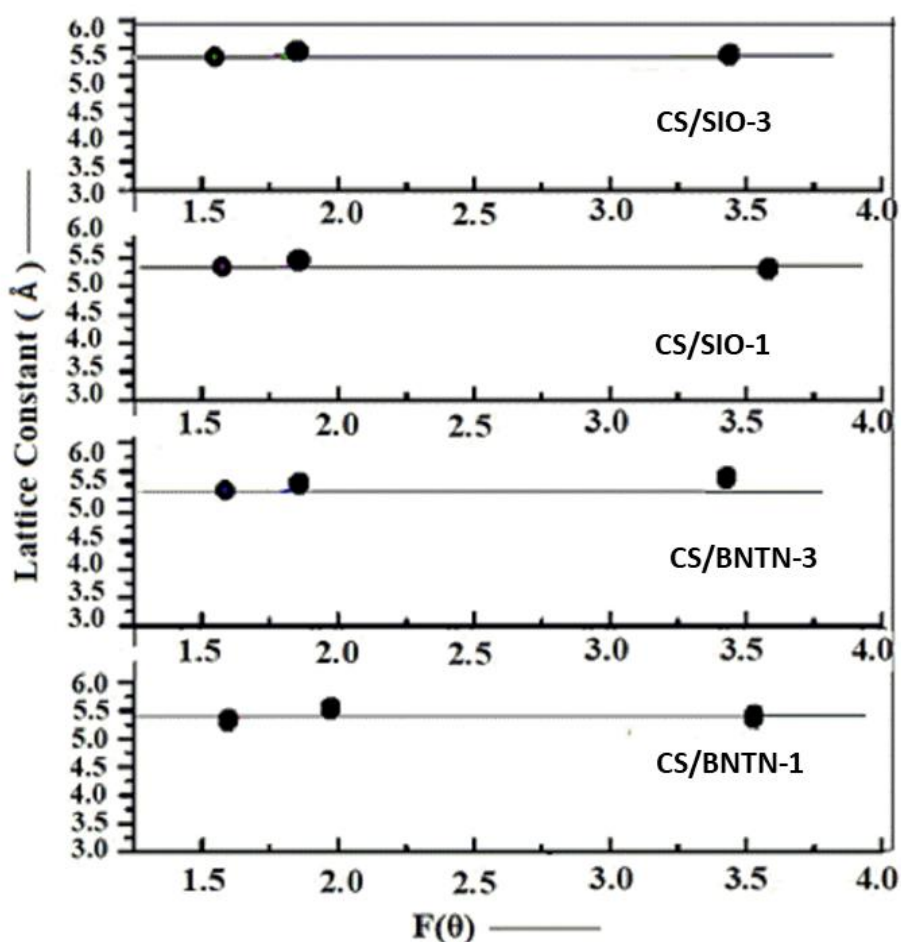


Figure 5.4. (b) Nelson and Riley graphs for biocomposite films containing CS and clay.

5.3.2.2. Analysis via SEM

To understand and visualize the morphologies of the synthesized CS/clay biocomposite films, SEM images were recorded. Figure 5.5. shows the micrographs which illustrate the morphological changes of the biocomposite films. SEM micrograph of the biocomposites shows in which manner the clay particles are incorporated into the CS molecules. Additionally, the distribution of the clay particles throughout the CS molecule is observed. For CS/BNTN biocomposite films, an increase in the clay amount results in a more rugged structure. The homogeneous dispersion of the clay particles proves the presence of an exfoliated structure [79]. Analysis of Figure 5.5.(a) and 5.5.(b) reveals that the CS/BNTN biocomposite films have a uniform appearance with small irregularities and bumps. In the case of CS/SIO biocomposite films, the SEM images are shown in Figure 5.5.(c) and 5.5.(d)

which shows that the biocomposite films have a rough and irregular surface [51] and a flocculated fraction of SIO is observed. It is observed that the biocomposite films exhibit considerable flocculation and intercalated morphology. The hydroxylated edge-edge interaction of the silicate layers causes the formation of a flocculated structure in the biocomposite films [69]. Chapter 4 discussed the SEM micrographs of CS and CS/KAO biocomposite films where it was observed that with an increase in the amount of KAO clay in the biocomposite, the surface becomes rougher. By analyzing the SEM images of all the biocomposite films, the surface of the CS/KAO biocomposite films was found to be smoother and more uniform than those of the CS/BNTN and CS/SIO biocomposite films. According to the structure of CS, it possesses one amino group and two hydroxyl functional groups. The silicate layers and matrix are thought to interact strongly because it is expected that the hydroxylated silicate edge groups and the functional groups of CS can form hydrogen bonds. The results indicate that CS is intercalated over the clay particles [39].

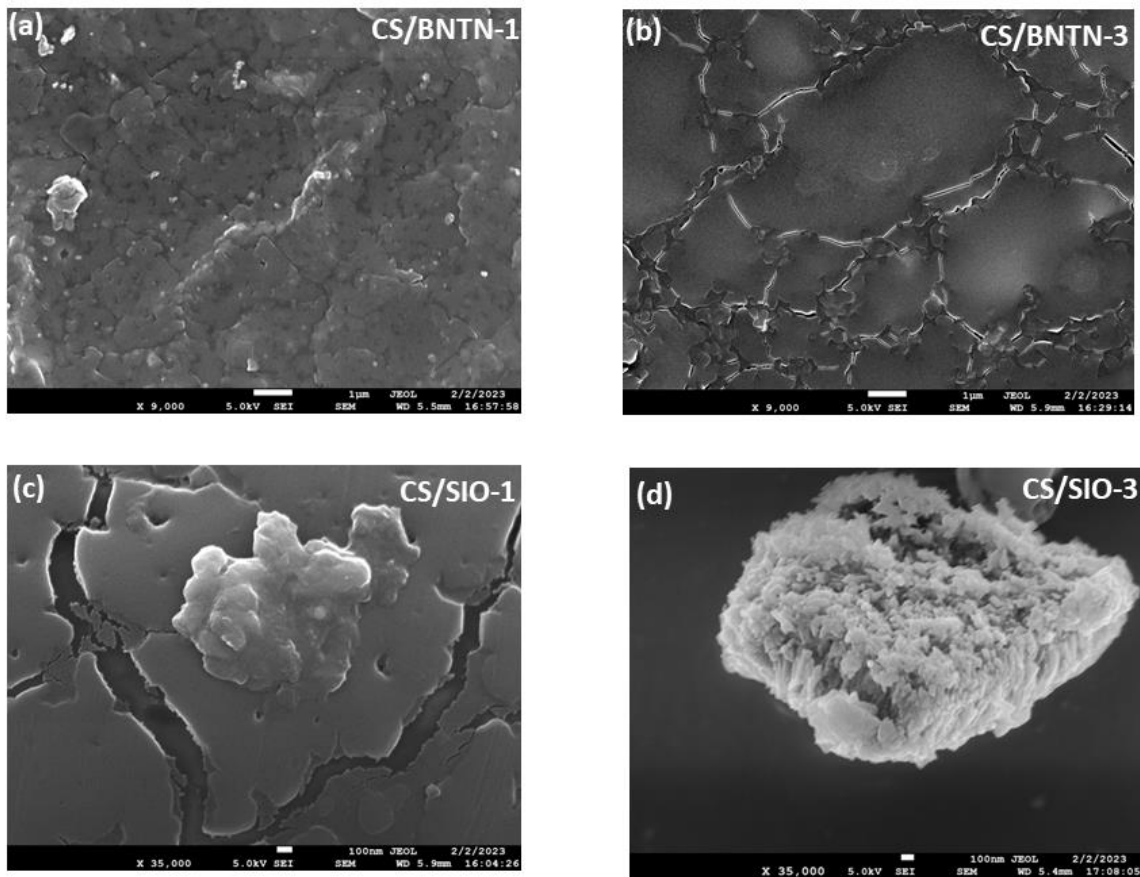


Figure 5.5. SEM micrographs of (a) CS/BNTN-1 (b) CS/BNTN-3 (c) CS/SIO-1 and (d) CS/SIO-3.

5.3.3. Mechanical property

The literature survey prevails that researchers have given much importance to the development of CS/clay biocomposites intending to use them for some specific kind of applications where good mechanical properties are not a requirement. However, one of the key qualities that can separate polymers from tiny molecules is often found to be their mechanical properties. The mechanical properties such as elongation at break and tensile strength are examined to gain more knowledge of the physical properties of CS/clay biocomposite films. In Table 5.2. both characteristics are listed. It has been shown that when the number of clay particles in biocomposite film rises, the elongation at break reduces but the tensile strength improves. Lin *et al.* [77] and Laaraibi *et al.* [78] also observed similar trends in the addition of BNTN clay to the CS matrix. In comparison to CS/KAO and CS/SIO biocomposite films, it is noted that CS/BNTN biocomposite films possess the highest tensile strength. A high tensile strength value indicates an increase in the stiffness of the biocomposite film whereas low elongation at break result shows that decrease in ductility. The finding indicates that CS/BNTN-3 possesses the highest stiffness and lowest ductile properties among all synthetic biocomposite films. These properties indicate that CS/BNTN-3 has higher brittleness characteristics. Thus, the fragility order of the synthesized biocomposite films is as follows:

$$\text{CS/BNTN-3} > \text{CS/BNTN-1} > \text{CS/KAO-3} > \text{CS/KAO-1} > \text{CS/SIO-3} > \text{CS/SIO-1}$$

The higher tensile strength of CS/clay biocomposite films indicates an improved polymer-filler interaction. The high tensile strength of CS/clay biocomposite films, an intriguing mechanical characteristic, makes them attractive options for use as a food packaging material.

Table 5.2. Tensile properties of various CS/clay biocomposite films.

Biocomposite films	Elongation at break (%)	Tensile Strength (in N)
CS/KAO-1	5.8 ± 0.1	55.1 ± 2.2
CS/KAO-3	5.5 ± 0.1	58.5 ± 2.4
CS/BNTN-1	5.2 ± 0.2	94.3 ± 3.1
CS/BNTN-3	4.3 ± 0.1	96.2 ± 3.3
CS/SIO-1	5.5 ± 0.2	37.9 ± 1.2
CS/SIO-3	5.2 ± 0.2	40.2 ± 1.3

5.3.4. Thermal analysis

5.3.4.1. TGA

To investigate the thermal stability of the material, TGA of the CS/clay biocomposite films is performed. Figure 5.6. shows the TGA plots for the CS/clay biocomposite films. The plots show that the degradation processes for the biocomposite films took place in two steps. In the case of CS/BNTN biocomposite films, the first degradation range (50-200 °C) is related to the loss of water, while the second breakdown occurs at about 280 °C for CS/BNTN-1 and about 287 °C for CS/BNTN-3 which represents the deacetylation and degradation of CS and the final stage which occurs in the vicinity of 450–550 °C can be assumed to be related to the oxidative breakdown of the carbon-based residue produced during the preceding stage. The results thus obtained are well agreed with the TGA data obtained by Laaraibi *et al.* in their investigation [78]. For CS/SIO biocomposite films, the first stage of degradation is observed at a temperature below 120 °C, which can be considered as evaporation of water. The second stage observed at 200-350 °C indicates the breakdown of the organic components of the CS/SIO biocomposite films and the third stage at the range of about 370-590 °C. These showed the high stability exhibited by the biocomposite films, composed of CS and SIO clay. The results show close agreement with the results obtained by the Salama *et al.* in their report [91]. Chapter 4 revealed the thermal stability of CS and CS/KAO biocomposite films where we explored that the CS/KAO biocomposites have superior thermal stability than the pure CS and also on increasing the clay proportion in the biocomposite, there was a clear enhancement in the stability of CS/KAO biocomposite films. Herein, we have explored that the thermal stability of the biocomposite films progressively rises as the clay percentage increases and that the decomposition temperature of CS/BNTN and CS/SIO biocomposite films display greater thermal stability than the pure CS. The temperature ranges at which synthesized CS/clay biocomposite films degrade are listed in Table 5.3. On comparing the outcomes with chapter 4 which is based on the CS/KAO biocomposite films, it has been noticed that the CS/SIO biocomposite films exhibited a slightly higher thermal stability than the CS/BNTN biocomposite films and the CS/BNTN biocomposite films exhibited slightly greater than those of CS/KAO biocomposite films. The high melting point of SIO clay, which has the ability to withstand very high temperatures without suffering substantial degradation, and BNTN clay, which can sustain moderately high temperatures without suffering vital degradation, are thought to be causes of this order. The KAO clay, on the other hand, undergoes a phase transformation as the temperature rises.

Table 5.3. Thermal properties of CS/clay biocomposite films.

Sample	1 st breakdown		2 nd breakdown	
	T _{onset} (°C)	T _{max} (°C)	T _{onset} (°C)	T _{max} (°C)
CS/BNTN-1	219	280	450	545
CS/BNTN-3	227	287	460	550
CS/SIO-1	200	343	370	565
CS/SIO-3	216	350	378	570

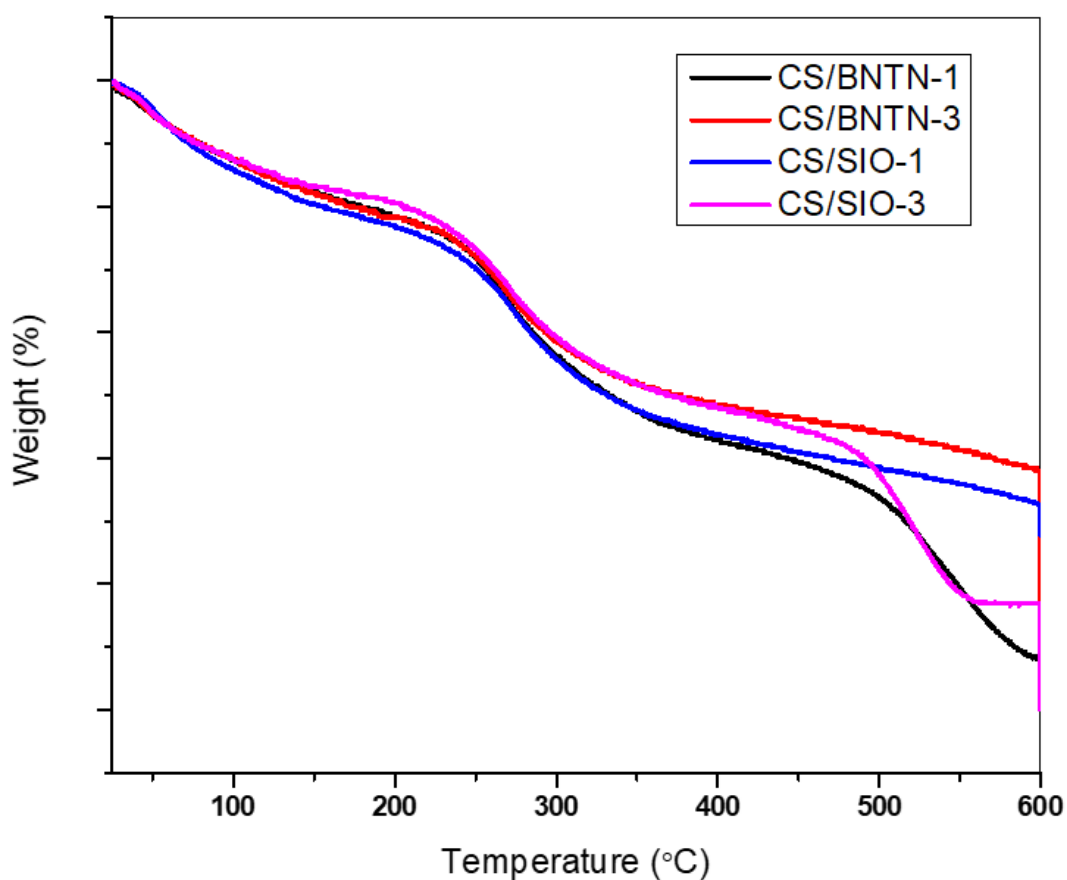


Figure 5.6. TGA graphs for different biocomposite films comprising CS and clay.

5.3.4.2. Analysis via DSC

As shown in Figure 5.7., thermograms obtained from DSC for the CS/BNTN and CS/SIO biocomposite films provided some substantial results. Chapter 4 reported that the CS degrades exothermically in the temperature range between 328-329 °C, whereas CS/KAO biocomposite films degrade between 340-343 °C. Herein, the degradation peak was obtained

for CS/BNTN biocomposite films in the temperature range between 347-349 °C, whereas the peak for CS/SIO biocomposite films was obtained between 350-353 °C. The result indicates that the degradation of biocomposite films was delayed because of their interaction with the particles of clay. As a consequence, the thermal stability of CS/clay biocomposite films was enhanced distinctly. The thermal stability order of all three types of biocomposite films is as follows:

$$\text{CS/SIO} > \text{CS/BNTN} > \text{CS/KAO}$$

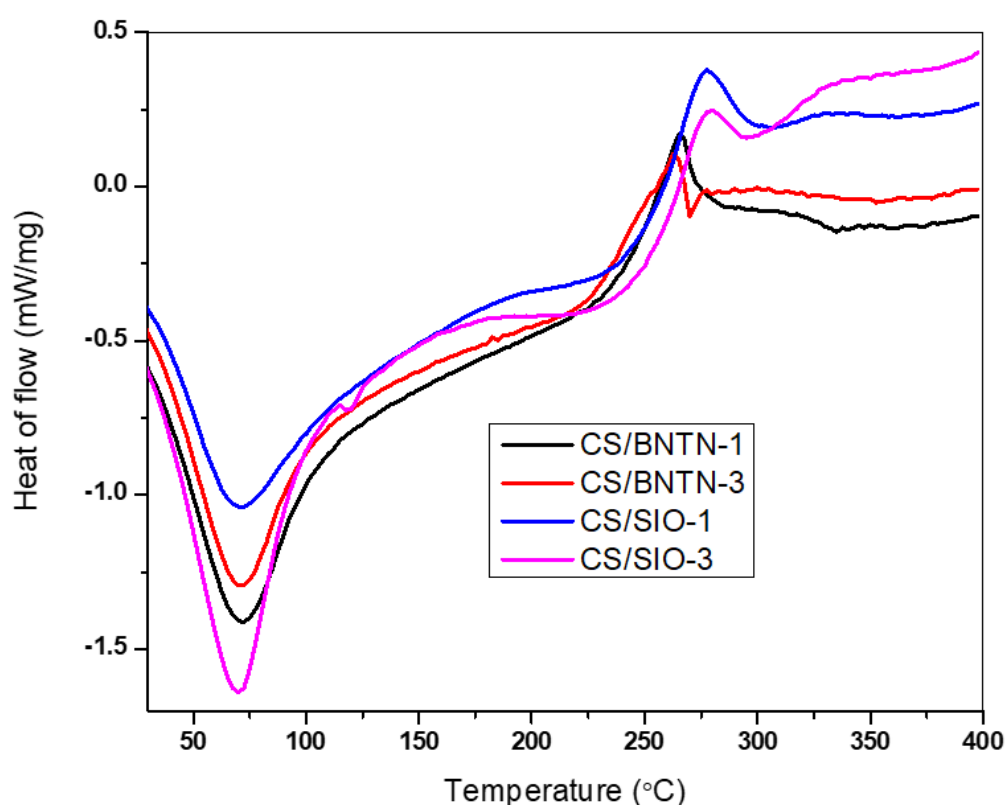


Figure 5.7. DSC thermograms of different CS/clay biocomposite films.

5.3.5. Study of antibacterial property

The agar well diffusion procedure for antimicrobial analysis [98] of the CS/clay biocomposite films is shown in Figure 5.8. At a concentration of 10 mg mL⁻¹, the antimicrobial activity of the test samples i.e., CS/BNTN-1, CS/BNTN-3, CS/SIO-1, and CS/SIO-3, were assessed against *Escherichia coli* and *Bacillus subtilis*. With respect to *Escherichia coli*, CS/BNTN-3 showed the largest zone of inhibition, measuring up to 26 mm in diameter, followed by CS/BNTN-1 with 25 mm, CS/SIO-3 with 24 mm and CS/SIO-1 with 23 mm. In case of *Bacillus subtilis*, CS/BNTN-3 showed the maximum zone of

inhibition, measuring up to 23 mm, followed by CS/BNTN-1 and CS/SIO-3 with 22 mm and CS/SIO-1 with 21 mm.

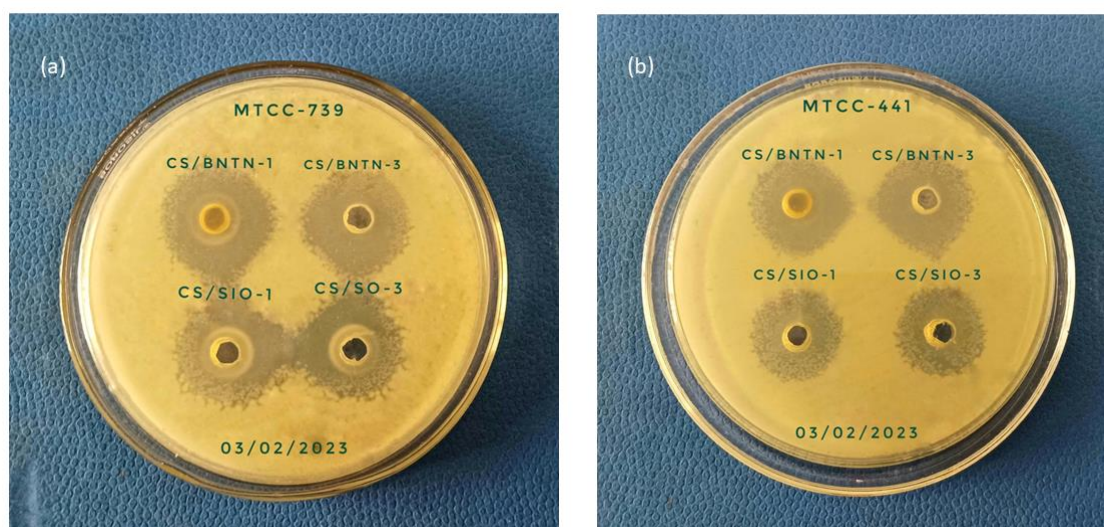


Figure 5.8. Antimicrobial activities showing zone of inhibition by CS/clay biocomposite films against (a) *Escherichia coli* and (b) *Bacillus subtilis*.

The obtained antimicrobial results were compared with the published article of CS/KAO biocomposite films reported in chapter 4. It is observed that a significant zone of inhibition in millimetres (mm) among the three combinations of CS/clay biocomposite films is as follows:

$$\text{CS/BNTN} > \text{CS/SIO} > \text{CS/KAO}$$

Our literature review revealed that the agar well diffusion method has never been used to evaluate the antimicrobial effects of CS/SIO biocomposite films. In the current investigation, all of the biocomposite films demonstrate measurable inhibitory effects against both gram negative and gram-positive bacteria. Cankaya *et al.* have reported the antibacterial characteristics of CS/Na⁺ Montmorillonite and CS/Nanoclay, highlighting their significant antimicrobial efficacy in these biocomposite materials [79]. Vijayalekshmi *et al.* also investigated the antibacterial activity of CS-Montmorillonite Clay/TiO₂ nanocomposites using gram negative and gram positive bacteria and observed all the nanocomposite shows high antibacterial activity [151].

Table 5.4. summarizes the zone of inhibition of crude extract against bacterial strains MTCC-739 and MTCC-441.

Table 5.4. Zone of inhibition in a test against bacterial strains MTCC-739 and MTCC-441.

Sl. No.	Test sample	Zone of inhibition (diameter) mm	
		<i>Escherichia coli</i> bacteria (MTCC-739)	<i>Bacillus subtilis</i> bacteria (MTCC-441)
1.	CS/BNTN-1	25 ± 0.02	22 ± 0.02
2.	CS/BNTN-3	26 ± 0.01	23 ± 0.01
3.	CS/SIO-1	23 ± 0.02	21 ± 0.02
4.	CS/SIO-3	24 ± 0.01	22 ± 0.01

5.3.6. Analysis of swelling test

All the synthesized CS/clay biocomposite films underwent swelling test analyses, and key findings are shown in Figure 5.9.

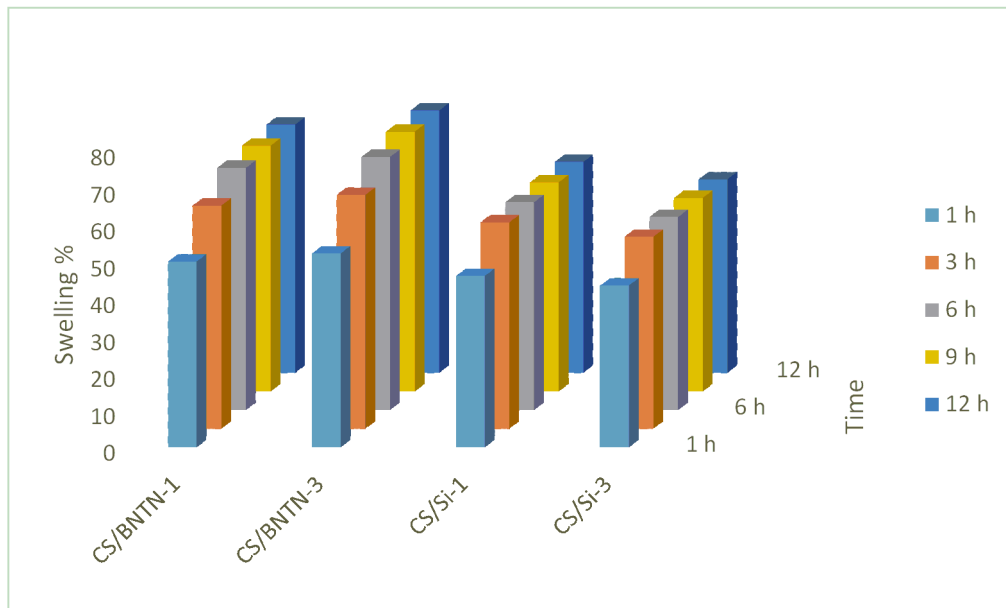


Figure 5.9. Plots of swelling test of various CS/clay biocomposite films.

All the findings thus obtained were compared with the investigation on CS and CS/KAO biocomposite films reported in chapter 4. The literature review reveals that no swelling test analysis for CS/SIO biocomposite films has been reported. Herein, it is found that the swelling capacity of CS/BNTN biocomposite films increases with time along with an increase in BNTN clay content. In comparison to pure CS film, these biocomposite films exhibit enhanced swelling characteristics. The reason for this change may be assumed to be the structural correlation between CS and BNTN clay. The water absorption capacity of CS

rises with an increase in the concentration of BNTN clay, which provides additional sites for water to interact, as a result, the biocomposite films swell more [84]. Abdelkrim *et al.* reported similar results with BNTN clay [152]. On the other hand, CS/SIO biocomposite films exhibit some interesting results that are quite similar to those of CS/KAO clay biocomposite films. The analysis reveals that the swelling property of the biocomposite films has an inverse relationship to the addition of SIO clay to the CS matrix. The hydrophilic properties offered by the $-NH_2$ and $-OH$ groups present within the CS, which provide some interactions with the clay particles, can be used to explain this property. The percentages of swelling for synthesized CS/clay biocomposite films are summarized in Table 5.5. From the analysis, it is clear that CS/BNTN-3 exhibited the highest swelling characteristics.

Table 5.5. Swelling % of various CS/clay biocomposite films.

Sample type	% of Swelling				
	1 h	3 h	6 h	9 h	12 h
CS/BNTN-1	50.2	60.3	65.5	66.4	67.1
CS/BNTN-3	52.4	63.2	68.4	70.2	70.9
CS/SIO-1	46.3	55.8	56.2	56.5	57
CS/SIO-3	43.7	51.9	52.2	52.3	52.3

5.4. Conclusion

The prepared CS/clay biocomposite films were characterized via FT-IR, UV/Vis, XRD, SEM, UTM, TGA and DSC analyses. FT-IR and UV-Vis analyses show the interactions between CS and clay particles in the prepared biocomposite revealing the successful preparation of biocomposite rather than a physical mixture. XRD and SEM analyses provide the necessary information about the distribution of clay particles in the CS molecule. CS/BNTN biocomposite films show a bit more complicated crystalline structure than the CS/SIO biocomposite films. SEM micrographs indicate an intercalated kind of morphology exhibited by both types of biocomposite films. For all the biocomposite films, an improvement in mechanical properties has been observed. Compared to CS/SIO and CS/KAO biocomposite films, CS/BNTN biocomposite films have a higher tensile strength. The thermal stability of all the biocomposite films was remarkable. The CS/SIO biocomposite films were found to have better thermal stability than CS/BNTN and CS/SIO

biocomposite films. Antimicrobial activity results reveal that both gram-negative and gram-positive bacterial growth are strongly inhibited by all of the biocomposite films. Additionally, CS/BNTN biocomposite film exhibits the highest zone of inhibition against both types of bacteria. Among the synthesized biocomposite films, CS/BNTN-3 exhibits good mechanical and significant antimicrobial properties than the other two. Therefore, it is assumed that CS/BNTN-3 would be an excellent candidate for food packaging material.